BIOCHEMISTRY
including biophysical chemistry & molecular biology

Article

pubs.acs.org/biochemistry

Investigating the Structural Variability and Binding Modes of the Glioma Targeting NFL-TBS.40−63 Peptide on Tubulin

Yoann Laurin,[†] Philippe Savarin,[‡] Charles H. Robert,[†] Masayuki Takahashi,[§] Joel Eyer,[∥] Chantal Prevost,[†] and Sophie Sacquin-Mora*[,†]

[†]Laboratoire de Biochimie Théorique, UPR 9080 CNRS Institut de Biologie Physico-Chimique,13 rue Pierre et Marie Curie, 75005 Paris, France

[‡]Université Paris 13, Sorbonne Paris Cité, CSPBAT, UMR 7244 CNRS, 74 rue Marcel Cachin, 93017 Bobigny, France

[§]School of Bioscience and Biotechnology, Tokyo Institue of Technology 2-12-1-M6-14 Ookayama, Meguro-ku, Tokyo 152-8550 Japan

[∥]Laboratoire de Neurobiologie & Transgenèse, UPRES EA 3143, INSERM, Centre Hospitalier Universitaire, Angers, France

Supporting Information

ABSTRACT: NFL-TBS.40−63 is a 24 amino acid peptide corresponding to the tubulin-binding site located on the light neurofilament subunit, which selectively enters glioblastoma cells, where it disrupts their microtubule network and inhibits their proliferation. We investigated its structural variability and binding modes on a tubulin heterodimer using a combination of NMR experiments, docking, and molecular dynamics (MD) simulations. Our results show that, while lacking a stable structure, the peptide preferentially binds on a specific single site located near the β-tubulin C-terminal end, thus giving us precious hints regarding the mechanism of action of the NFL-TBS.40−63 peptide's antimitotic activity at the molecular level.

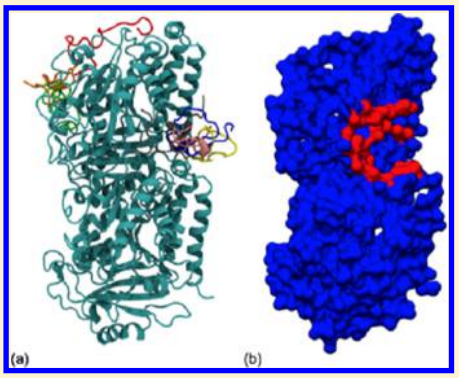

Tubulin is a structural protein whose α/β heterodimer forms the basic building blocks of microtubules (MT). Each of the α- and β-tubulin subunits consists of multiple isotypes differing in amino acid sequence and encoded by different genes.[1] Tubulins are arranged in a head-to-tail fashion to form around 13 protofilaments that together constitute cylindrical MTs with an outer diameter of around 25 nm. Microtubules coexist in growing and shrinking populations, and this dynamic instability is essential for their biological activity since MTs are cytoskeletal components that are critically involved in several key cellular processes such as mitosis, intracellular transport, or cell motility.[2]

As a consequence for cancer chemotherapy, tubulin is the target of some of the most successful antitumor drugs, such as taxanes, the vinca alkaloids, or colchicinoids.[3−5] After cellular uptake, most cytotoxic drugs will target the microtubule network since it plays an essential role for chromatid separation during meiosis. Antimitotic compounds will interfere with microtubule dynamics by inhibiting the polymerization or depolymerization of α,β-tubulin dimers into microtubules, thus inhibiting cancer cell division and proliferation.[3,6] For example, paclitaxel (Taxol) binding to MTs alters their dynamic properties and leads to the stabilization of MTs against depolymerization.[7] Vinblastine (a member of the vinca alkaloids family), however, will destabilize microtubules and inhibit tubulin polymerization.[8]

While it is known that most clinically used tubulin binding agents target the β-tubulin subunit of the α/β heterodimer, an important issue, which is still, by and large, left unanswered, concerns the tubulin isotypes which should be specifically targeted in cancer chemotherapy.[9] The ultimate goal being to design drugs that will preferentially bind the overexpressed tubulin isotype and therefore be lethal to cancer cells only, leaving normal cells intact. Indeed, recent studies have demonstrated that glioblastomas, which are the most common primary brain tumors, exhibit significant changes in their MT cytoskeleton,[10] including aberrant expression of the class III β-tubulin isotype and γ-tubulin, which are associated with the emergence of highly malignant tumor phenotypes. Furthermore, the increase in βIII microtubules has been shown to be associated with paclitaxel resistance,[11−14] thus making the selective targeting of specific tubulin isotypes a key issue for anticancer drug design.

Three interconnected structures compose the neuronal cytoskeleton: actin microfilaments, microtubules, and intermediate filaments (IFs). Recently, the neurobiology group of J. Eyer performed *in vitro* and *in vivo* experiments showing that IF proteins bind unpolymerized tubulin and suggested a model in

Received: February 12, 2015
Revised: April 30, 2015
Published: May 27, 2015

DOI: 10.1021/acs.biochem.5b00146
Biochemistry 2015, 54, 3660−3669

which IFs act as a reservoir modulating the local availability of tubulin throughout the axon.[14] Their research showed that conserved sites, called tubulin-binding sites (TBS), present in the N-terminal domain of all three NF subunits, are capable of mediating the interaction between tubulin and assembled NFs. Although peptides corresponding to these conserved sequences have no effect on the stability of already assembled MTs, they inhibit MT polymerization *in vitro*. Furthermore, these peptides can enter cells in culture, thus leading to disruption of the MT cytoskeleton and altered cell proliferation. In contrast, peptides in which the amino acid sequence has been reversed or scrambled lose these properties.

Of all TBS containing peptides examined so far, NFL-TBS.40−63, which is derived from the light neurofilament protein (NFL), demonstrates the highest capacity to inhibit microtubule formation in an *in vitro* polymerization assay.[14] Further studies on this peptide have shown that *in vitro*, it is more efficiently internalized by glioma cells than by normal cells, this difference not being species specific.[15] Moreover, once internalized by glioma cells, the peptide strongly affected their microtubule network, attenuated proliferation, and led to apoptosis, a cell death mechanism shared by many cancer cells when treated with antimitotic drugs.[16] Also, it is thought that glioblastoma motility relies on microtubules, and consistent with this notion, noncytotoxic concentrations of Taxol and Vinca alkaloids can impede their migration.[17,18] Similarly, a noncytotoxic concentration of the NFL-TBS.40−63 peptide was found to attenuate glioblastoma migration.[15] These *in vitro* properties of the NFL-TBS.40−63 peptide were also observed *in vivo*, when the peptide was injected into the brains of glioma-bearing rats. All considered, this peptide appears to be a remarkable candidate for malignant glioma treatment.

Following a first structure−function analysis of the NFL-TBS.40−63 peptide alone, which combined alanine scanning, circular dichroism measurements, and molecular modeling of the peptide's structure,[19] we present additional structural data resulting from NMR experiments and molecular dynamics (MD) simulations. Furthermore, we investigated the peptide's interaction with tubulin, using a combination of docking and MD simulations. Our calculations show that, despite its high structural variability, the peptide preferentially binds on β-tubulin, in the vicinity of the external stathmin binding-site. These results provide us with precious information regarding the mechanism of action of the NFL-TBS.40−63 peptide's antimitotic activity at the molecular level.

MATERIALS AND METHODS

Peptide Synthesis. The peptide was synthesized with biotine by Millegen, Labege, France with a minimal 98% purity. The purity and integrity of the peptide were verified by mass spectrometry. The peptide was dissolved in water with the help of NH_4OH vapors.

NMR Spectroscopy. All ^1H NMR experiments were performed at 293 K on a Bruker Avance 600 MHz NMR spectrometer equipped with a cryoprobe. Data were processed using Topspin (Bruker). Sodium[3-trimethylsilyl-2,20,3,30-$2H_4$]-propionate (TSP-d4) was used as an internal reference for proton chemical shifts. Spectra of the peptide were collected at a peptide concentration of 1 mM in a H_2O/D_2O (90:10) mixture at pH 5. For sequence-specific assignments, two-dimensional (2D) DQF-COSY,[20] TOCSY,[21] NOESY,[22] and ROESY[23] spectra were used. The TOCSY experiments were acquired using the MLEV17 sequence[24] with a mixing time of 80 ms. In the NOESY experiments,[25] the mixing period was 200 ms. A mixing time of 100 ms was used to verify that spin diffusion is limited. The 2D ROESY spectrum was recorded with a mixing time of 300 ms. All 2D experiments were conducted with 2048 data points·512 increments·64 scans with a spectral width of 6000 Hz in both dimensions. The data were zero-filled to give a 4096·1024 data matrix prior to Fourier transformation. The NMR spectra were visualized and analyzed with NMRView version 5.0.4.[26]

Peptide Structural Modeling. Molecular modeling of the NFL-TBS.40−63 peptide structure was carried out using the PEP-FOLD program (Web server http://bioserv.rpbs.univ-paris-diderot.fr/services/PEP-FOLD/).[27,28] PEP-FOLD predicts "ab initio" the folding characteristics of peptides comprising 9 to 36 amino acids. It is based on structural alphabet SA letters describing the possible conformation of groups of four consecutive amino acids, which are selected and assembled via a genetic algorithm.[29] Structure reconstruction and energy evaluation rely on the coarse grain force field OPEP.[30] This program has been used successfully by several groups to predict biologically relevant peptide structures.[31−33] After this step, we kept the representative structures of the two most populated clusters (ranked third and eighth) for the remaining stages of the study.

Classical Molecular Dynamics on the Peptide and Tubulin Alone. Before docking the NFL-TBS.40−63 peptide on tubulin, each partner was submitted to classical molecular dynamics simulations in order to obtain a relaxed structure for tubulin and to produce a set of possible conformations from the two original peptide structures generated by PEP-FOLD in the previous stage. For tubulin, we used a straight dimer structure, corresponding to Protein Databank entry 1JFF,[34] in which paclitaxel, ions, and GDP/GTP were not taken into account, as a starting model. Note that the C-terminal tails from the α and β subunits (which respectively comprise 10 and 18 residues) do not appear in this crystal structure and were therefore excluded from our model, as usually done in previous molecular modeling studies of tubulin−ligand complexes.[13,35−39]

We used Gromacs version 4.6.3[40] with the OPLS-AA force field[41] in periodic boundary conditions to perform the simulations. The first step of the simulation procedure is an *in vacuo* minimization of the structure with the steepest descent algorithm during 1000 steps without any constraints. We added a water box of 1.2 nm, or 2 nm, around the peptide, or the tubulin, respectively, filled with TIP3P molecule type.[42] We then neutralized the system with the addition of ions randomly placed in the box while maintaining NaCl concentration at 150 mM. The final system comprises around 13 000 atoms for the tubulin heterodimer, 85 000 water molecules, and 500 ions (roughly half Na^+ and half Cl^-).

A minimization step was performed with the same set of parameters as before during 5000 steps to avoid possible water clashes with the molecule. After this stage, we made a two step equilibration procedure. The first step is in a NVT environment and the second one is in a NPT environment. Each stage of equilibration lasted 100 ps, with an integration step of 2 fs. The temperature was fixed at 300 K using the velocity rescale method.[43] All bonds were constrained with the LINCS algorithm,[44] and electrostatic interactions were computed using the Particle Mesh Ewald method.[45] For the pressure coupling during the NPT equilibration, we used the Parinello−Rahman method[46] at the value of 1 atm. Production phases were finally done using the same set of parameters and

DOI: 10.1021/acs.biochem.5b00146
Biochemistry 2015, 54, 3660−3669

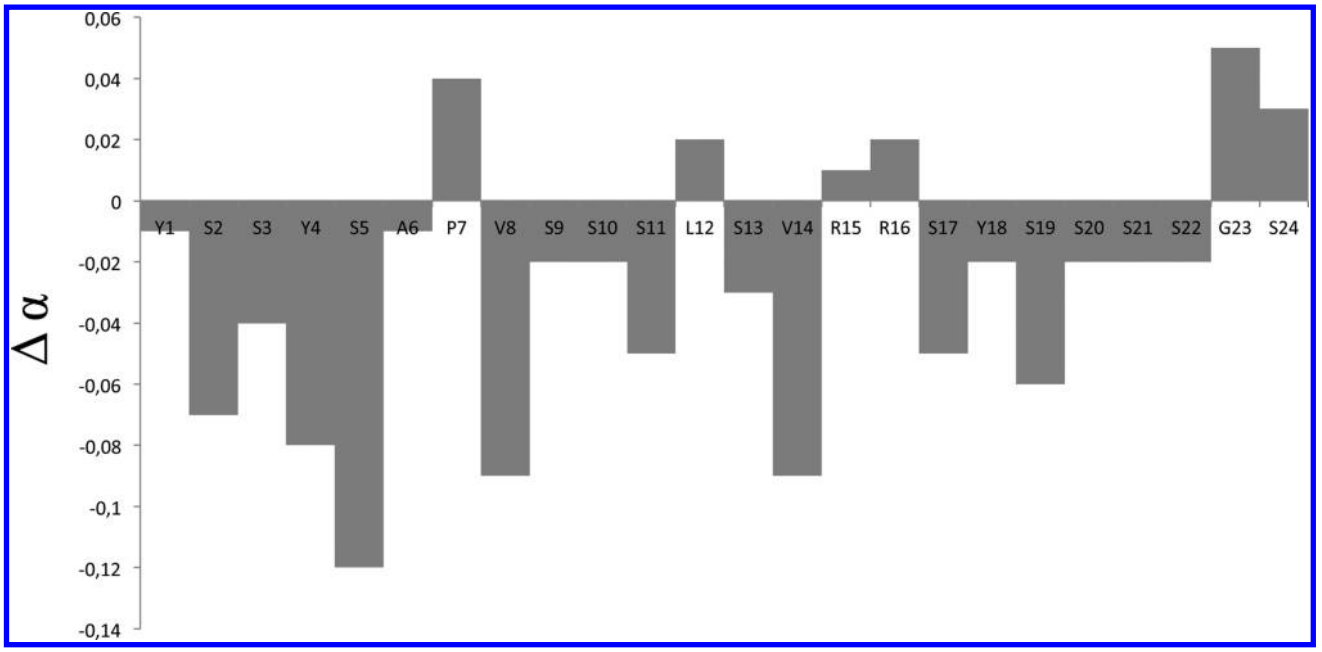

Figure 1. Peptide NFL-TBS.40−63 is fully disordered in solution. Variation of the α proton chemical shifts for the peptide in 90% H_2O/10% D_2O from random coil values. No successive significant deviations ($\Delta\ \alpha < -0.1$ ppm or >0.1 ppm), that would reveal the presence of secondary structures, are observed.

algorithms during 50 ns. Trajectories were saved every 10 ps, and the analyses were made on the last 45 ns, considering the initial 5 ns as an equilibration period.

After obtaining the trajectories, we processed them with the Gromacs utilities and VMD[47] for the visual part. We clustered the structures resulting from the 45 ns production period using the Gromos algorithm[48] with the RMSD (root mean square deviation) cutoff at 5 Å for the peptide and 1.5 Å for the tubulin, these cutoffs being chosen according to the average RMSDs that were observed during the simulations, which are much larger for the peptide than for the tubulin heterodimer (see Figure SI1a-b, Supporting Information). Because of its remarkable structural stability, we kept only one representative structure of the most populated cluster for the tubulin. For the peptide, we chose to keep seven representative structures of the most populated clusters produced by the two MD simulations that were then docked on tubulin during the next stage of our study. In addition, the peptide structural variability and secondary structure evolution during the MD runs were analyzed with the DSSP tool.[49]

Docking Calculations. To perform the coarse-grain rigid-body docking step between tubulin and NFL-TBS.40−63 peptide, we used PTools/ATTRACT suite[50,51] with the structures chosen before, with the tubulin as the fixed receptor and the peptide as the mobile ligand. ATTRACT uses a multiple energy minimization algorithm (with the L-BGFS minimizer, which is a quasi-Newton minimizer for solving nonlinear optimization problems[52,53]), starting from several positions and orientations of the ligand that are distributed on a grid all around the receptor protein. This grid is calculated with a modified Shrake and Rupley algorithm,[54] so that every point is located at 10 Å of its neighbors, and the distance between the ligand and the receptor's surface is the square of the ligand protein's radius. The number of ligand starting positions depends on the receptor size (around 270−300 points in our case), and there are around 250 starting ligand orientations for each starting position. No experimental data are used to restrict the conformational search during energy minimization, and the ATTRACT protocol comprises a series of four successive minimizations using decreasing cutoffs for the calculation of the interaction pairlist.[51] For each docking procedure, the ensemble of resulting docking poses was then processed with the PTools built-in clustering algorithm with a 1 Å cutoff for the RMSD criterion. We retained one docked position for each of the seven starting ligand structures, which is the representative structure of the most energetically favorable cluster.

Classical Molecular Dynamics on the Peptide−Tubulin Complex. After visually assessing the docking positions on the tubulin with VMD, we performed a second stage of molecular dynamic simulation on the complete system (i.e., peptide + tubulin) . The same procedure as before the docking step was used for the simulation, but the production phase was now 100 ns long instead of 50 ns. Analyses of the results were done using Gromacs utilities, VMD, and a homemade Python script using the PTools library.

RESULTS

NMR Spectroscopy on the NFL-TBS.40−63 Peptide Shows It Is Mostly Disordered in Solution. The NMR structure of the free peptide with biotine at the N-terminal was investigated at pH 5. Despite numerous superpositions, resulting from the high number of serine residues in the peptide sequence, the proton resonances were assigned at 294 K by means of TOCSY and NOESY spectra using the Wüthrich method.[55] The values of the chemical shifts for the Hα protons, which are sensitive to the secondary structure, correspond to random coil structure.[56] Consequently, the peptide does not adopt any predominant regular secondary structure (see Figure 1). This was confirmed by the NOESY assignment. 171 NOEs were observed but correspond essentially to intraresidue or sequential connectivities (86% intra or sequential, 11% middle range, and 3% long-range). These results are in agreement with the CD spectra that were previously observed in pure water.[19]

DOI: 10.1021/acs.biochem.5b00146
Biochemistry 2015, 54, 3660−3669

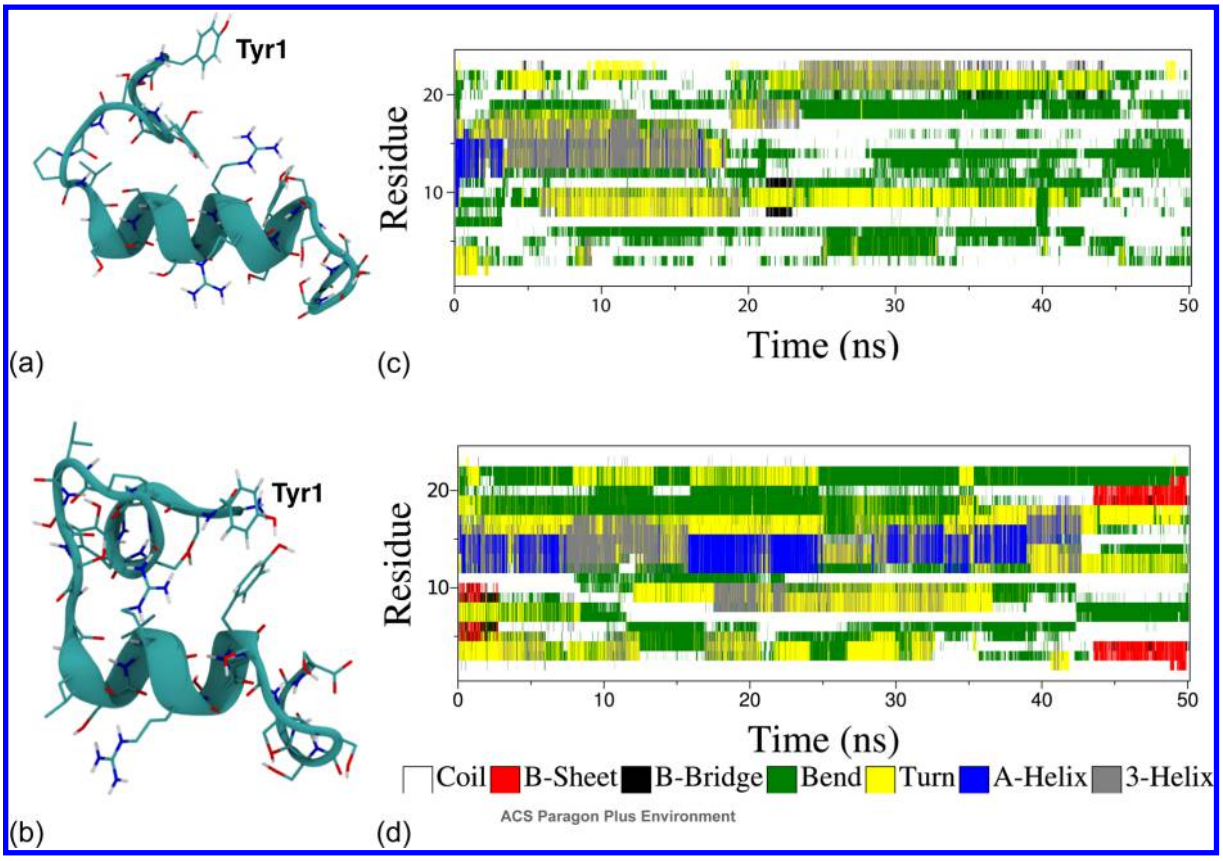

Figure 2. (a,b) NFL-TBS.40−63 (YSSYSAPVSSSLSVRRSYSSSSGS) peptide representative structures of the two most populated structural clusters generated by PEP-FOLD. (c,d) DSSP graphs from the MD simulations made with the peptide structures shown in a and b, respectively.

The peptide (400 μM) was also studied in the presence of tubulin (60 μM), and a strong aggregation was then observed.

Structural Predictions for the NFL-TBS.40−63 Peptide and Tubulin Alone. *NFL-TBS.40−63 Peptide.* As the folding of the peptide could not be observed by NMR experiments, we tried to model it using the PEP-FOLD program, which produced 163 structural clusters for the NFL-TBS.40−63 peptide, only two of which (ranked third and eight among the best predictions with score of −18.18 and −16.81 kJ mol^{-1}, respectively) were composed of three structures. This is a first indication of the peptide's high structural variability.

Two representative structures from these clusters are shown in Figure 2a,b and were retained for the following MD simulations of the isolated peptide. Both structures are basically formed by an α-helix core surrounded by unstructured fragments on each extremity.

The RMSD plots resulting from MD simulations of these two structures, and shown in Figure SI1b (Supporting Information), highlight their lack of stability and the potential reorganization of their secondary structure along the trajectory. Root mean square fluctuations (RMSF) calculations on the peptides' main chain atoms (see Figure SI1c, Supporting Information) lead to similar results, showing important structural fluctuations even for the initially helical core. We also used DSPP to assign secondary structure elements during the MD simulations, thus highlighting the essentially unstructured nature of the peptide, with most of its amino acids being in a coil or turn conformation (see Figure 2c,d and Table 1)

The use of the Gromos clustering tool on the two trajectories led to the selection of four and three most populated structural clusters, which represent 80% and 95% of the trajectory, respectively (see Table 2 for a summary). The seven representative structures issued from these clusters are shown in Figure 3 and will be referred to later as pep1 to pep7 (pep1 to pep4 being clusters produced by the first simulation and pep5 to pep7 being produced by the second simulation). These structures were used as a starting point for the rigid-body docking calculations of the peptide on tubulin. As we can see in Figure 3, these structures are mostly disordered, in agreement with the DSSP[57] assignments shown in Figure 2c,d. Some still present an α-helix fragment in their core, while two (pep2 and pep6) present a β-hairpin fold. These results are in agreement with the structural data that was obtained via molecular

Table 1. Secondary Structure Attribution for the NFL-TBS.40−63 Peptide during MD Simulations (from DSSP)

	coil	helix	sheet	bend	turn
PEP-FOLD cluster 3	51%	9%	1%	27%	12%
PEP-FOLD cluster 8	36%	15%	2%	26%	20%

Table 2. Peptide Structural Clusters Selected for Docking on Tubulin

PEP-FOLD cluster	cluster 3				cluster 8		
Gromos cluster	pep1	pep2	pep3	pep4	pep5	pep6	pep7
structures	2447	839	472	310	3154	1140	477
% of trajectory	48.9	16.8	8.4	6.2	63.1	22.8	9.5
	80.3				95.4		

DOI: 10.1021/acs.biochem.5b00146
Biochemistry 2015, 54, 3660−3669

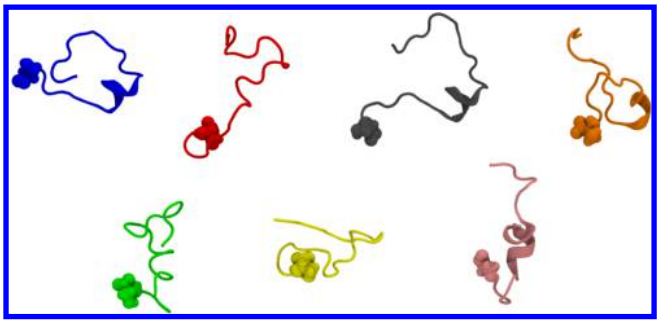

Figure 3. Seven selected peptide structures from the MD simulations. From left to right, first row, pep1 to pep4; second row, pep5 to pep7. The C-terminal residue is shown as van der Waals spheres.

modeling and circular dichroism experiments in a previous work on the NFL-TBS.40−63 peptide,[19] and with the NMR experiments described earlier in this article.

Tubulin. The tubulin dimer is extremely stable during the all-atom MD simulation, as can be seen in Figure SI1a (Supporting Information). Structural clustering led to the production of a representative structure issued from the most populated cluster (which accounts for roughly 20% of the trajectory) and shown in Figure 4a. The surface electrostatic potential for this

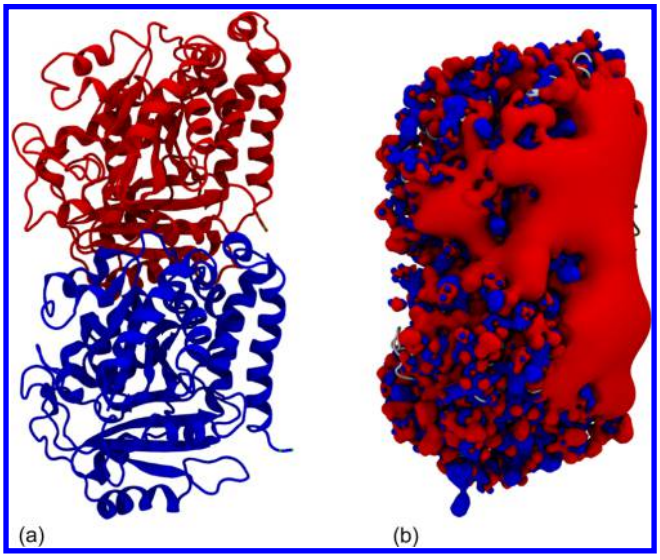

Figure 4. Tubulin structure before peptide docking. (a) Cartoon representation of the tubulin heterodimer with the α-subunit in blue and the β-subunit in red. (b) Surface electrostatic potential resulting from APBS calculations. Positive potentials are shown in blue and negative ones in red.

structure was then calculated with APBS and is shown in Figure 4b. The tubulin heterodimer presents an important electronegative groove in the vicinity of the subunit's C-terminal regions, which are the exposed parts of the protein when it is embedded into a microtubule superstructure.

Coarse-Grain Rigid-Body Docking of the Peptide on the Tubulin Heterodimer. *Peptide Native Sequence Docking.* The rigid-body docking calculations lead to docking poses with binding energy that are comprised between −5 kcal·mol^{-1} and −10.5 kcal·mol^{-1} (for the most favorable structures), values that are similar to those obtained in previous docking calculations of small ligands on tubulin.[36,38,39] For each one of the peptide's seven starting structures, the docking poses resulting from the ATTRACT procedure were clustered using the RMSD as a criterion. Figure 5a shows a representative

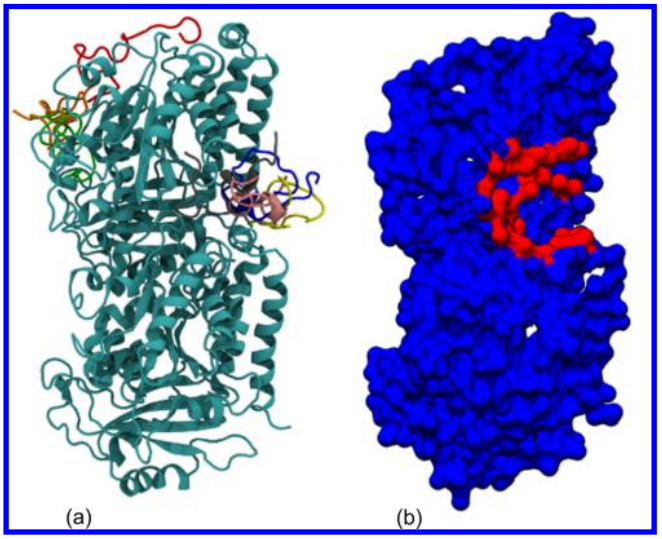

Figure 5. Docking the NFL-TBS.40−63 peptide in the tubulin heterodimer. (a) Best docking position for each of the seven peptide structures shown in Figure 3 (the color-code has been conserved). (b) Mapping the tubulin−peptide interaction energy from all the docking calculations; high affinity (i.e., low energy) sites are shown in red, while low affinity (i.e., high energy) sites are in blue. The affinity is calculated as the energy-weighted probability of a tubulin surface atom being involved in a docked interface.

position on the tubulin for the best cluster associated with each of the seven original peptide structures. Similarly to most tubulin associated molecules (either proteins or small ligands), the NFL-TBS.40−63 peptide essentially binds on the heterodimer's β-subunit. We also mapped on the tubulin surface an average interaction energy taking into account each tubulin's residue's participation in all of the docking poses, following the new Ptools protocol introduced in ref 58. That is, for each tubulin surface residue, we calculate the probability of this residue being involved in a docked interface generated during the ATTRACT procedure, and this probability is weighted by the interaction energies resulting from the coarse-grain potential.

As we can see in Figures 5b and SI2 (Supporting Information), this leads to the highlighting of a preferential binding spot located in the vicinity of the outer electrostatic groove mentioned earlier. This external cavity, which is located near the two β-subunit C-terminal helices, hosts four out of the seven best docking poses generated by ATTRACT (for structures pep1, pep3, pep6, and pep7). The three remaining best docking poses are on the other side of the tubulin β-subunit, either near the taxol luminal site (for structures pep4 and pep5) or on top of the tubulin near the vinblastin binding site (pep2). However, these three peptide structures (pep2, pep4, and pep5) do also present docking poses with favorable (if not the best) energies in the common external cavity, thus enhancing its weight in the mapping statistics leading to Figure 5b.

Scrambling the Peptide's Sequence. A similar procedure (PEP-FOLD structural prediction + MD simulations + docking on tubulin) was applied to a peptide with a composition identical with the NFL-TBS.40−63 but where the amino-acid sequence has been scrambled (corresponding to the NFL-

DOI: 10.1021/acs.biochem.5b00146
Biochemistry 2015, 54, 3660−3669

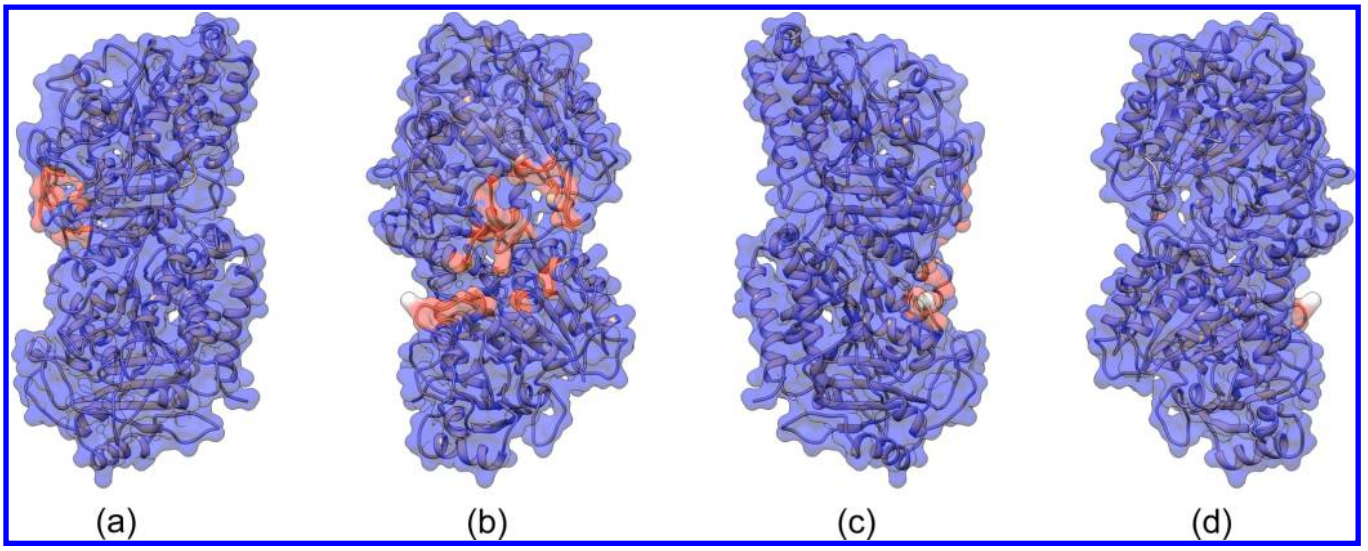

Figure 6. Mapping the interaction energy between tubulin and the scrambled peptide, four views rotating around the vertical axis. The tubulin orientation in panel a and the color code are the same as those in Figure 5b.

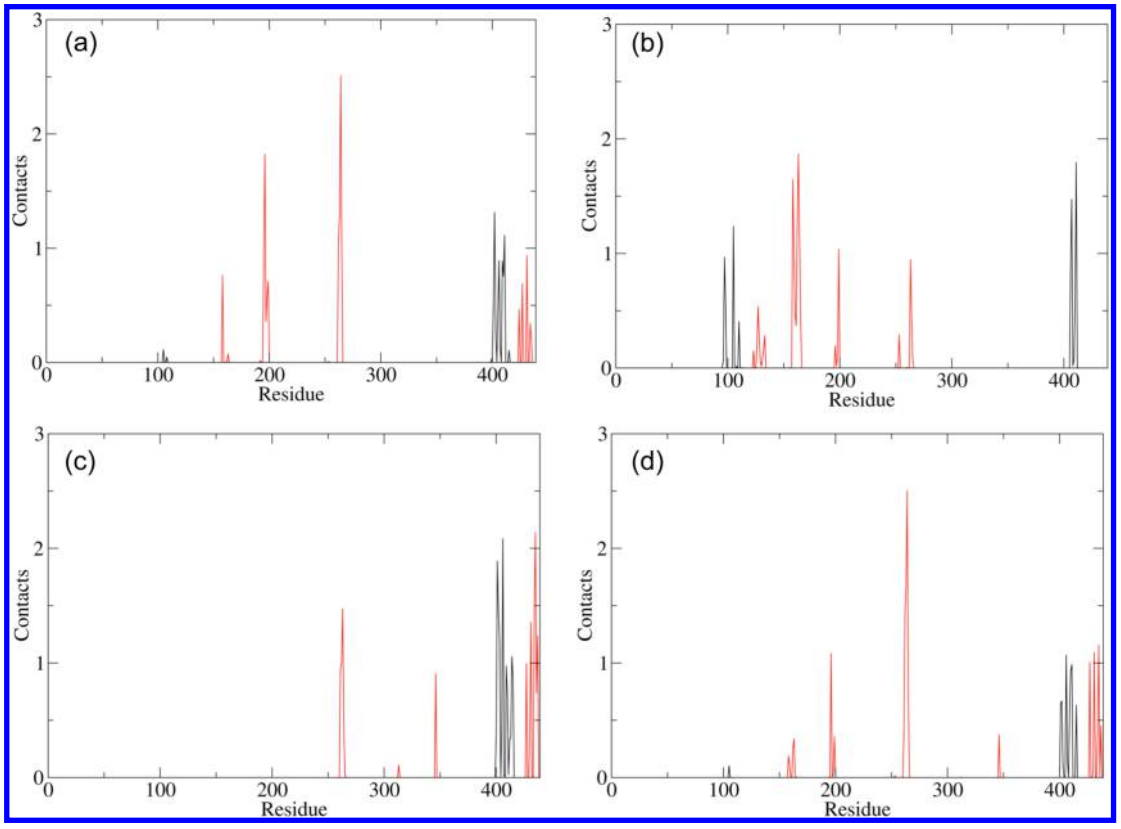

Figure 7. Average number of contacts between tubulin residues and the four peptide structures, (a) pep1, (b) pep3, (c) pep6, and (d) pep7, during the postdocking MD simulations. Black line: contacts between the peptide and the α-subunit. Red line: contacts between the peptide and the β-subunit.

SCR1 sequence in ref 14). Again, MD simulations of the scrambled peptide highlight its lack of a preferential secondary structure, with important RMSDs in a range (but slightly lower) similar to that for the NFL-TBS.40−63 peptide (see Figure SI3, Supporting Information). However, the docking pattern on the tubulin heterodimer for this scrambled peptide is quite different from the one obtained with the original NFL sequence (see Figure 6) with most peptides now bound in the vicinity of the taxol luminal site that is on the opposite side of the binding site for the native sequence peptides. We can also note how the regions that favorably bind the scrambled peptide are more scattered over the tubulin surface and show less pronounced affinity compared to that of the binding site of the original peptide.

Postdocking Molecular Dynamics. Following the docking procedure, for the four peptide structures that were located in the preferential binding spot (i.e., pep1, pep3, pep6, and pep7), we performed a second MD simulation step on the

DOI: 10.1021/acs.biochem.5b00146
Biochemistry 2015, 54, 3660−3669

complete system (tubulin heterodimer and bound peptide) in order to investigate how peptide binding can impact the tubulin structure, dynamics, and mechanical properties. The RMSD for the complex is shown in Figure SI4a (Supporting Information) and does not reveal any noticeable changes compared with those of the tubulin heterodimer alone. The peptide, however, presents lower RMSDs than in its unbound state (Figure SI4b, Supporting Information), as could be expected. The RMSFs show a considerable increase in stability compared with that of the unbound peptide for the residues located on the interface with the tubulin: that is, central residues for pep1, pep3, and pep7, and the terminal residues of pep6; see Figure SI4c (Supporting Information). On the time scale of our simulations, we did not observe any convergence of the four peptidic structures toward a common conformation or any reptation of the peptide on the tubulin's surface.

We investigated the peptide and tubulin residues forming contacts during the simulations, according to the CAPRI standards,[59] i.e., heavy atoms less than 4 Å away from each others; see Figure 7 and Table SI1 (Supporting Information). Interestingly, the tubulin contact pattern is similar to that of the four peptides, notwithstanding the different peptidic structures. In particular, residues 400−415 from the α-subunit H11 and 255−265 from the β-subunit appear in all four contact patterns from Figure 6, while residues 155−165, 195−200, 340−345, and 415−435 (corresponding to the H11 helix) from the β-subunit appear in at least two out of the four contact patterns.

DISCUSSION

Peptide Structure. The results from the PEP-FOLD calculations and NMR experiments are consistent with our previous observations using modeling and circular dichroism experiments[19] that the NFL-TBS.40−63 peptide does not present a stable and well-defined conformation in solution. In this perspective, PEP-FOLD might not be the most adapted tool since it does not aim at capturing the structural characteristics of disordered peptides. It is, however, a useful tool to generate starting peptide structures that were then refined during the MD simulations stage. Our results regarding the peptide lack of a stable structure are in agreement with the fact that it is derived from the N-terminal head domain of the NFL protein, which is also unstructured and interacts with the tail and central rod domains during the formation of protofilaments.[60−62]

Peptide Docking on Tubulin. Despite its high structural variability, NFL-TBS.40−63 clearly presents a preferential binding-site located in the vicinity of the outer electronegative groove on the surface of the tubulin heterodimer. We can also note that the binding of various peptidic structural forms on this specific location makes this interaction even more favorable from the free energy point of view. Interestingly, this external cavity is not one of the classical binding sites usually encountered for antimitotic tubulin binding drugs such as taxol, vinblastin, or colchicin and which are located on the luminal site or on the interface between the α and β-subunits.[4] The peptide binding site presents more common points with MAP (microtubule associated protein) binding sites that were previously identified for motor proteins such as kinesin[2,3,63−65] or dynein,[66] or for structural MAPs which modulate microtubule stability in the cell such as stathmin,[6] MAP65,[67] tau, or MAP2.[68] Furthermore, our external binding site concurs with the binding site hypothesis of Saidi Brikci-Nigassa et al.[69] for the interaction of the connexin C-terminal domain, another 26 amino-acids peptide derived from a protein involved in signal transduction, on tubulin that was proposed following NMR experiments and the coarse-grain docking simulation. Finally, peptides bound to this external site also lay close to the β-subunit's C-terminal end. The β-subunit C-terminal tail, which has a length of 18 residues (β427−444), does not appear in the original crystallographic structure that was used for our simulations (1JFF) and was therefore not modeled during our study. It is highly flexible, negatively charged, and is thought to play a critical role in regulating MT assembly.[2,70−75] Remarkably, in a recent simulation work,[76] Freedman et al. have shown how the β C-terminal tail can present an intermonomer mode of interaction pairing its charged residues with α-H11 from a neighboring tubulin. When binding on the external site of the tubulin heterodimer, NFL-TBS.40−63 might not only hinder the C-terminal tail mobility but also interfere with the MT assembly process, thus providing an interpretation for the experimental observations by Bocquet et al.[14] that the peptide can inhibit MT polymerization *in vitro* (while having no effect on the stability of assembled MTs). Furthermore, residues α-Lys 401 (from helix H11), β-Trp346 (from the H10/B9 loop), β-Asp 427, and Glu 431, which are listed as residues involved in the inter- and intradimer contacts mediated by the C-terminal tail,[76] figure in the peptide contact patterns shown in Figure 7. The binding of the NFL-TBS.40−63 peptide could therefore prevent the formation of several contacts between the β-C-terminal tail and tubulin, thus once again inhibiting MTs formation. Figure 8 shows a close-up view

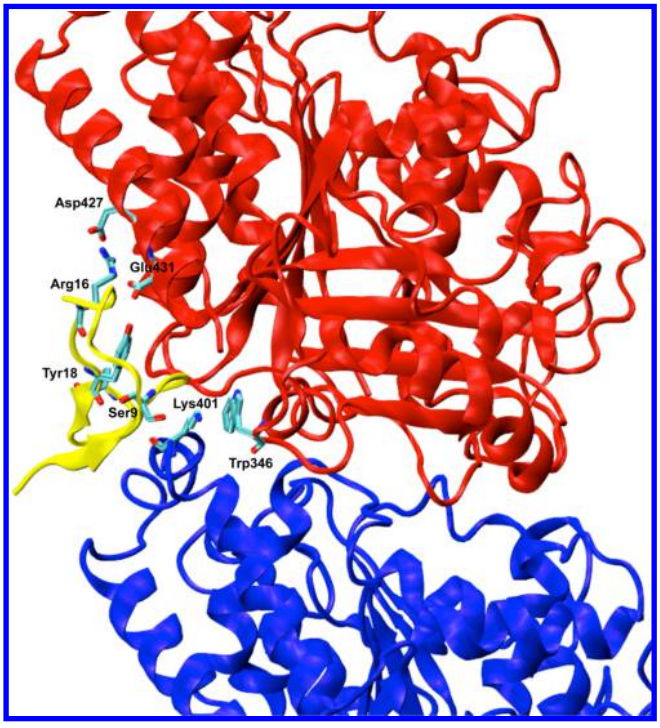

Figure 8. Close-up view of the interaction between pep6 (in yellow) and tubulin (the α-subunit in blue and the β-subunit in red).

of the interaction between the peptide structure pep6 and tubulin during the post docking simulation. It is interesting to note that the peptide residues forming contacts with the aforementioned tubulin residues are Ser9, Arg16, and Tyr18, which were shown to have a key role during cell uptake and MT disruption via alanine scanning experiments.[19] Arg16 in

DOI: 10.1021/acs.biochem.5b00146
Biochemistry 2015, 54, 3660−3669

particular seems to be playing a crucial part in the peptide's activity since Arg16Ala mutants lose all their cell penetration capacity.

In addition to these perturbations of tubulin intra- and intercontacts, the bound peptide is also likely to impede the interactions between tubulin and MAPs in charge of regulating the dynamics of MT assembly, which would also contribute to the disruption of the cytoskeleton network that was observed in living cells.[15]

The fact that the NFL-SCR1 peptide, which has the same composition as NFL-TBS.40−63 but with a scrambled sequence, presents a totally different binding pattern on the tubulin heterodimer is also noteworthy since this NFL-SCR1 peptide was shown experimentally to have a much lower capacity to affect the MT network in cells.[14] Despite its structural variability, the sequence of NFL-TBS.40−63 seems to be a key point for its binding on tubulin's outer surface.

CONCLUDING REMARKS

Using a combination of several modeling tools and NMR spectroscopy experiments, we investigated the structural variability and binding modes on the tubulin of NFL-TBS.40−63, a 24 amino-acid peptide derived from the light neurofilament subunit and which has been shown to disrupt MTs network and inhibit their proliferation *in vivo*. We show that the docking of several different peptide structures on a tubulin heterodimer leads to the identification of a common binding site located on the outer side of tubulin, near the β-subunit's C-terminal end. Our data suggest that the NFL-TBS.40−63 peptide binding on this site might hinder MT formation and its dynamic regulation in the cell, by impeding the β C-terminal tail mobility, preventing important intra- and interdimer contacts within MTs and interfering with MAPs that usually bind on the MT's outer-side.

Future work will investigate the selective action of the NFL-TBS.40−63 peptide on glioma cells by specifically modeling its interaction with class III β-tubulin isotypes, which are known to be overexpressed in several tumor types.[77] In particular, it is interesting to note that most sequence differences between the βI and βIII-tubulin isotypes are indeed located in the C-terminal tail,[74] which now appears to be a key part of the protein if we want to further understand the interaction mode of the NFL-TBS.40−63 peptide with tubulin and which will have to be properly modeled in later simulations (using the original works of Luchko et al.[78] and Freedman et al.[76] as a starting point). Because of the important flexibility of the C-terminal tails, our rigid-body docking approach is no longer suitable to investigate the tubulin/NFL-peptide system and will have to be modified in further studies to account for the tail's mobility during the docking procedure. The fact that the C-terminal tails are subject to many post-translational modifications (such as tyrosination, glutamylation, glycilation, or phosphorylation)[1,79,80] represents another simulation challenge since all these chemical changes are known to impact the structure and dynamics of the C-termini and therefore the MT formation process.

Finally, since resistance to usual tubulin binding agents, such as paclitaxel, has been related to the overexpression of the βIII isoform of β-tubulin,[8,11−13] the development of a new compound with high affinity for this specific tubulin isotype would, in a long-term perspective, help clinicians to tailor therapies with optimized tumor response and survival.

ASSOCIATED CONTENT

Supporting Information

Peptide and tubulin conformational details and structural data (RMSD and RMSF) from the MD simulations. The Supporting Information is available free of charge on the ACS Publications website at DOI: 10.1021/acs.biochem.5b00146.

AUTHOR INFORMATION

Corresponding Author

*E-mail: sacquin@ibpc.fr.

Funding

Y.L. wishes to thank the "Initiative d'Excellence" program from the French State (Grant "DYNAMO", ANR-11-LABX-011-01) for doctoral funding.

Notes

The authors declare no competing financial interest.

REFERENCES

(1) Luduena, R. F. (1998) Multiple forms of tubulin: different gene products and covalent modifications. *Int. Rev. Cytol. 178*, 207−275.
(2) Aylett, C. H., Lowe, J., and Amos, L. A. (2011) New insights into the mechanisms of cytomotive actin and tubulin filaments. *Int. Rev. Cell. Mol. Biol. 292*, 1−71.
(3) Amos, L. A. (2011) What tubulin drugs tell us about microtubule structure and dynamics. *Semin. Cell Dev. Biol. 22*, 916−926.
(4) Dostal, V., and Libusova, L. (2014) Microtubule drugs: action, selectivity, and resistance across the kingdoms of life. *Protoplasma 251*, 991−1005.
(5) Massarotti, A., Coluccia, A., Silvestri, R., Sorba, G., and Brancale, A. (2012) The tubulin colchicine domain: a molecular modeling perspective. *ChemMedChem 7*, 33−42.
(6) Amos, L. A., and Schlieper, D. (2005) Microtubules and maps. *Adv. Protein Chem. 71*, 257−298.
(7) Jordan, M. A., Wendell, K., Gardiner, S., Derry, W. B., Copp, H., and Wilson, L. (1996) Mitotic block induced in HeLa cells by low concentrations of paclitaxel (Taxol) results in abnormal mitotic exit and apoptotic cell death. *Cancer Res. 56*, 816−825.
(8) Kavallaris, M. (2010) Microtubules and resistance to tubulin-binding agents. *Nat. Rev. Cancer 10*, 194−204.
(9) Tseng, C. Y., Mane, J. Y., Winter, P., Johnson, L., Huzil, T., Izbicka, E., Luduena, R. F., and Tuszynski, J. A. (2010) Quantitative analysis of the effect of tubulin isotype expression on sensitivity of cancer cell lines to a set of novel colchicine derivatives. *Mol. Cancer 9*, 131.
(10) Katsetos, C. D., Draberova, E., Legido, A., Dumontet, C., and Draber, P. (2009) Tubulin targets in the pathobiology and therapy of glioblastoma multiforme. I. Class III beta-tubulin. *J. Cell. Physiol. 221*, 505−513.
(11) Goncalves, A., Braguer, D., Kamath, K., Martello, L., Briand, C., Horwitz, S., Wilson, L., and Jordan, M. A. (2001) Resistance to Taxol in lung cancer cells associated with increased microtubule dynamics. *Proc. Nat. Acad. Sci. U.S.A. 98*, 11737−11742.
(12) Kamath, K., Wilson, L., Cabral, F., and Jordan, M. A. (2005) BetaIII-tubulin induces paclitaxel resistance in association with reduced effects on microtubule dynamic instability. *J. Biol. Chem. 280*, 12902−12907.
(13) Freedman, H., Huzil, J. T., Luchko, T., Luduena, R. F., and Tuszynski, J. A. (2009) Identification and characterization of an intermediate taxol binding site within microtubule nanopores and a mechanism for tubulin isotype binding selectivity. *J. Chem. Inf. Model. 49*, 424−436.
(14) Bocquet, A., Berges, R., Frank, R., Robert, P., Peterson, A. C., and Eyer, J. (2009) Neurofilaments bind tubulin and modulate its polymerization. *J. Neurosci. 29*, 11043−11054.
(15) Berges, R., Balzeau, J., Peterson, A. C., and Eyer, J. (2012) A tubulin binding peptide targets glioma cells disrupting their micro-

DOI: 10.1021/acs.biochem.5b00146
Biochemistry 2015, 54, 3660−3669

tubules, blocking migration, and inducing apoptosis. *Mol. Ther. 20*, 1367−1377.
(16) Wang, T. H., Wang, H. S., and Soong, Y. K. (2000) Paclitaxel-induced cell death: where the cell cycle and apoptosis come together. *Cancer 88*, 2619−2628.
(17) Terzis, A. J., Thorsen, F., Heese, O., Visted, T., Bjerkvig, R., Dahl, O., Arnold, H., and Gundersen, G. (1997) Proliferation, migration and invasion of human glioma cells exposed to paclitaxel (Taxol) in vitro. *Br. J. Cancer 75*, 1744−1752.
(18) Panopoulos, A., Howell, M., Fotedar, R., and Margolis, R. L. (2011) Glioblastoma motility occurs in the absence of actin polymer. *Mol. Biol. Cell 22*, 2212−2220.
(19) Berges, R., Balzeau, J., Takahashi, M., Prevost, C., and Eyer, J. (2012) Structure-function analysis of the glioma targeting NFL-TBS.40−63 peptide corresponding to the tubulin-binding site on the light neurofilament subunit. *PLoS One 7*, e49436.
(20) Rance, M., Sorensen, O. W., Bodenhausen, G., Wagner, G., Ernst, R. R., and Wuthrich, K. (1983) Improved spectral resolution in cosy 1H NMR spectra of proteins via double quantum filtering. *Biochem. Biophys. Res. Commun. 117*, 479−485.
(21) Braunschweiler, L., and Ernst, R. R. (1983) Coherence transfer by isotropic mixing - application to proton correlation spectroscopy. *J. Magn. Reson. 53*, 521−528.
(22) Kumar, A., Ernst, R. R., and Wuthrich, K. (1980) A two-dimensional nuclear Overhauser enhancement (2D NOE) experiment for the elucidation of complete proton-proton cross-relaxation networks in biological macromolecules. *Biochem. Biophys. Res. Commun. 95*, 1−6.
(23) Bax, A., and Davis, D. G. (1985) Practical aspects of two-dimensional transverse NOE spectroscopy. *J. Magn. Reson. 63*, 207−213.
(24) Bax, A., and Davis, D. G. (1985) MLEV-17-Based two-dimensional homonuclear magnetization transfer spectroscopy. *J. Magn. Reson. 65*, 355−360.
(25) Clore, G. M., and Gronenborn, A. M. (1982) Theory and applications of the transferred nuclear overhauser effect to the study of the conformations of small ligands bound to proteins. *J. Magn. Reson. 48*, 402−417.
(26) Johnson, B. A., and Blevins, R. A. (1994) NMR View: A computer program for the visualization and analysis of NMR data. *J. Biomol. NMR 4*, 603−614.
(27) Maupetit, J., Derreumaux, P., and Tuffery, P. (2009) PEP-FOLD: an online resource for de novo peptide structure prediction. *Nucleic Acids Res. 37*, W498−W503.
(28) Thevenet, P., Shen, Y., Maupetit, J., Guyon, F., Derreumaux, P., and Tuffery, P. (2012) PEP-FOLD: an updated de novo structure prediction server for both linear and disulfide bonded cyclic peptides. *Nucleic Acids Res. 40*, W288−293.
(29) Maupetit, J., Derreumaux, P., and Tuffery, P. (2010) A Fast method for large-scale de novo peptide and miniprotein structure prediction. *J. Comput. Chem. 31*, 726−738.
(30) Maupetit, J., Tuffery, P., and Derreumaux, P. (2007) A coarse-grained protein force field for folding and structure prediction. *Proteins 69*, 394−408.
(31) Duvignaud, J. B., Leclerc, D., and Gagne, S. M. (2010) Structure and dynamics changes induced by 2,2,2-trifluoro-ethanol (TFE) on the N-terminal half of hepatitis C virus core protein. *Biochem. Cell Biol. 88*, 315−323.
(32) Kawaguchi, A., Suzuki, T., Kimura, T., Sakai, N., Ayabe, T., Sawa, H., and Hasegawa, H. (2010) Functional analysis of an alpha-helical antimicrobial peptide derived from a novel mouse defensin-like gene. *Biochem. Biophys. Res. Commun. 398*, 778−784.
(33) Steckbeck, J. D., Craigo, J. K., Barnes, C. O., and Montelaro, R. C. (2011) Highly conserved structural properties of the C-terminal tail of HIV-1 gp41 protein despite substantial sequence variation among diverse clades. Implications for functions in viral replication. *J. Biol. Chem. 286*, 27156−27166.
(34) Lowe, J., Li, H., Downing, K. H., and Nogales, E. (2001) Refined structure of alpha beta-tubulin at 3.5 A resolution. *J. Mol. Biol. 313*, 1045−1057.
(35) Rendine, S., Pieraccini, S., and Sironi, M. (2010) Vinblastine perturbation of tubulin protofilament structure: a computational insight. *Phys. Chem. Chem. Phys. 12*, 15530−15536.
(36) Chakraborti, S., Chakravarty, D., Gupta, S., Chatterji, B. P., Dhar, G., Poddar, A., Panda, D., Chakrabarti, P., Ghosh Dastidar, S., and Bhattacharyya, B. (2012) Discrimination of ligands with different flexibilities resulting from the plasticity of the binding site in tubulin. *Biochemistry 51*, 7138−7148.
(37) Mane, J. Y., Semenchenko, V., Perez-Pineiro, R., Winter, P., Wishart, D., and Tuszynski, J. A. (2013) Experimental and computational study of the interaction of novel colchicinoids with a recombinant human alphaI/betaI-tubulin heterodimer. *Chem. Biol. Drug Des. 82*, 60−70.
(38) Liao, S. Y., Mo, G. Q., Chen, J. C., and Zheng, K. C. (2014) Exploration of the binding mode between (−)-zampanolide and tubulin using docking and molecular dynamics simulation. *J. Mol. Model. 20*, 2070.
(39) Banuelos-Hernandez, A. E., Mendoza-Espinoza, J. A., Pereda-Miranda, R., and Cerda-Garcia-Rojas, C. M. (2014) Studies of (−)-pironetin binding to alpha-tubulin: conformation, docking, and molecular dynamics. *J. Org. Chem. 79*, 3752−3764.
(40) Pronk, S., Pall, S., Schulz, R., Larsson, P., Bjelkmar, P., Apostolov, R., Shirts, M. R., Smith, J. C., Kasson, P. M., van der Spoel, D., Hess, B., and Lindahl, E. (2013) GROMACS 4.5: a high-throughput and highly parallel open source molecular simulation toolkit. *Bioinformatics 29*, 845−854.
(41) Kaminski, G. A., Friesner, R. A., Tirado-Rives, J., and Jorgensen, W. L. (2001) Evaluation and reparametrization of the OPLS-AA force field for proteins via comparison with accurate quantum chemical calculations on peptides. *J. Phys. Chem. B 105*, 6474−6487.
(42) Jorgensen, W. L., Chandrasekhar, J., Madura, J. D., Impey, R. W., and Klein, M. L. (1983) Comparison of simple potential functions for simulating liquid water. *J. Chem. Phys. 79*, 926−935.
(43) Bussi, G., Donadio, D., and Parrinello, M. (2007) Canonical sampling through velocity rescaling. *J. Chem. Phys. 126*, 014101.
(44) Hess, B., Bekker, H., Berendsen, H. J. C., and Fraaije, J. (1997) LINCS: A linear constraint solver for molecular simulations. *J. Comput. Chem. 18*, 1463−1472.
(45) Essmann, U., Perera, L., Berkowitz, M. L., Darden, T., Lee, H., and Pedersen, L. G. (1995) A smooth particle mesh Ewald method. *J. Chem. Phys. 103*, 8577−8593.
(46) Parrinello, M., and Rahman, A. (1981) Polymorphic transitions in single crystals: A new molecular dynamics method. *J. Appl. Phys. 52*, 7182−7190.
(47) Humphrey, W., Dalke, A., and Schulten, K. (1996) VMD: visual molecular dynamics. *J. Mol. Graphics 14* (33−38), 27−38.
(48) Daura, X., Gademann, K., Jaun, B., Seebach, D., van Gunsteren, W. F., and Mark, A. E. (1999) Peptide folding: When simulation meets experiment. *Angew. Chem., Int. Ed. 38*, 236−240.
(49) Touw, W. G., Baakman, C., Black, J., Te Beek, T. A., Krieger, E., Joosten, R. P., and Vriend, G. (2011) A series of PDB-related databanks for everyday needs. *Nucleic Acids Res. 39*, D411−D419.
(50) Saladin, A., Fiorucci, S., Poulain, P., Prevost, C., and Zacharias, M. (2009) PTools: an opensource molecular docking library. *BMC Struct. Biol. 9*, 27.
(51) Schneider, S., Saladin, A., Fiorucci, S., Prevost, C., and Zacharias, M. (2012) ATTRACT and PTools: open source programs for protein-protein docking. *Methods Mol. Biol. 819*, 221−232.
(52) Nocedal, J. (1980) Updating quasi-Newton matrices with limited storage. *Math. Comput. 35*, 773−782.
(53) Liu, D. C., and Nocedal, J. (1989) On the limited memory BFGS method for large-scale optimization. *Math. Program. 45*, 503−528.
(54) Shrake, A., and Rupley, J. A. (1973) Environment and exposure to solvent of protein atoms. Lysozyme and insulin. *J. Mol. Biol. 79*, 351−371.

DOI: 10.1021/acs.biochem.5b00146
Biochemistry 2015, 54, 3660−3669

(55) Wüthrich, K. (1986) *NMR of Proteins and Nucleic Acids*, Wiley, New York.
(56) Wishart, D. S., and Sykes, B. D. (1994) The 13C chemical-shift index: a simple method for the identification of protein secondary structure using 13C chemical-shift data. *J. Biomol. NMR 4*, 171−180.
(57) Baker, N. A., Sept, D., Joseph, S., Holst, M. J., and McCammon, J. A. (2001) Electrostatics of nanosystems: application to microtubules and the ribosome. *Proc. Natl. Acad. Sci. U.S.A. 98*, 10037−10041.
(58) Boyer, B., Ezelin, J., Poulain, P., Saladin, A., Zacharias, M., Robert, C. H., and Prevost, C. (2015) An integrative approach to the study of filamentous oligomeric assemblies, with application to RecA. *PLoS One 10*, e0116414.
(59) Janin, J. (2005) Assessing predictions of protein-protein interaction: the CAPRI experiment. *Protein Sci. 14*, 278−283.
(60) Geisler, N., Kaufmann, E., Fischer, S., Plessmann, U., and Weber, K. (1983) Neurofilament architecture combines structural principles of intermediate filaments with carboxy-terminal extensions increasing in size between triplet proteins. *EMBO J. 2*, 1295−1302.
(61) Fuchs, E., and Weber, K. (1994) Intermediate filaments: structure, dynamics, function, and disease. *Annu. Rev. Biochem. 63*, 345−382.
(62) Perrot, R., and Eyer, J. (2009) Neuronal intermediate filaments and neurodegenerative disorders. *Brain Res. Bull. 80*, 282−295.
(63) Goulet, A., Major, J., Jun, Y., Gross, S. P., Rosenfeld, S. S., and Moores, C. A. (2014) Comprehensive structural model of the mechanochemical cycle of a mitotic motor highlights molecular adaptations in the kinesin family. *Proc. Natl. Acad. Sci. U.S.A. 111*, 1837−1842.
(64) Shang, Z., Zhou, K., Xu, C., Csencsits, R., Cochran, J. C., and Sindelar, C. V. (2014) High-resolution structures of kinesin on microtubules provide a basis for nucleotide-gated force-generation, *eLife 3*.
(65) Cao, L., Wang, W., Jiang, Q., Wang, C., Knossow, M., and Gigant, B. (2014) The structure of apo-kinesin bound to tubulin links the nucleotide cycle to movement. *Nat. Commun. 5*, 5364.
(66) Carter, A. P., Garbarino, J. E., Wilson-Kubalek, E. M., Shipley, W. E., Cho, C., Milligan, R. A., Vale, R. D., and Gibbons, I. R. (2008) Structure and functional role of dynein's microtubule-binding domain. *Science 322*, 1691−1695.
(67) Subramanian, R., Wilson-Kubalek, E. M., Arthur, C. P., Bick, M. J., Campbell, E. A., Darst, S. A., Milligan, R. A., and Kapoor, T. M. (2010) Insights into antiparallel microtubule crosslinking by PRC1, a conserved nonmotor microtubule binding protein. *Cell 142*, 433−443.
(68) Al-Bassam, J., Ozer, R. S., Safer, D., Halpain, S., and Milligan, R. A. (2002) MAP2 and tau bind longitudinally along the outer ridges of microtubule protofilaments. *J. Cell Biol. 157*, 1187−1196.
(69) Saidi Brikci-Nigassa, A., Clement, M. J., Ha-Duong, T., Adjadj, E., Ziani, L., Pastre, D., Curmi, P. A., and Savarin, P. (2012) Phosphorylation controls the interaction of the connexin43 C-terminal domain with tubulin and microtubules. *Biochemistry 51*, 4331−4342.
(70) Serrano, L., de la Torre, J., Maccioni, R. B., and Avila, J. (1984) Involvement of the carboxyl-terminal domain of tubulin in the regulation of its assembly. *Proc. Natl. Acad. Sci. U.S.A. 81*, 5989−5993.
(71) Sackett, D. L., Bhattacharyya, B., and Wolff, J. (1985) Tubulin subunit carboxyl termini determine polymerization efficiency. *J. Biol. Chem. 260*, 43−45.
(72) Serrano, L., Wandosell, F., de la Torre, J., and Avila, J. (1988) Effect of specific proteolytic cleavages on tubulin polymer formation. *Biochem. J. 252*, 683−691.
(73) Wolff, J., Sackett, D. L., and Knipling, L. (1996) Cation selective promotion of tubulin polymerization by alkali metal chlorides. *Protein Sci. 5*, 2020−2028.
(74) Joe, P. A., Banerjee, A., and Luduena, R. F. (2009) Roles of beta-tubulin residues Ala428 and Thr429 in microtubule formation in vivo. *J. Biol. Chem. 284*, 4283−4291.
(75) Yadav, S., Verma, P. J., and Panda, D. (2014) C-terminal region of MAP7 domain containing protein 3 (MAP7D3) promotes microtubule polymerization by binding at the C-terminal tail of tubulin. *PLoS One 9*, e99539.
(76) Freedman, H., Luchko, T., Luduena, R. F., and Tuszynski, J. A. (2011) Molecular dynamics modeling of tubulin C-terminal tail interactions with the microtubule surface. *Proteins 79*, 2968−2982.
(77) Katsetos, C. D., Draberova, E., Legido, A., Dumontet, C., and Draber, P. (2009) Tubulin targets in the pathobiology and therapy of glioblastoma multiforme. I. Class III beta-tubulin. *J. Cell. Phys. 221*, 505−513.
(78) Luchko, T., Huzil, J. T., Stepanova, M., and Tuszynski, J. (2008) Conformational analysis of the carboxy-terminal tails of human beta-tubulin isotypes. *Biophys. J. 94*, 1971−1982.
(79) Luduena, R. F. (2008) *The Role of Microtubules in Cell Biology, Neurobiology, and Oncology* (Fojo, T., Ed.), pp 105−121, Humana Press, Totowa, NJ.
(80) Roll-Mecak, A. (2015) Intrinsically disordered tubulin tails: complex tuners of microtubule functions? *Semin. Cell Dev. Biol. 37*, 11−19.

DOI: 10.1021/acs.biochem.5b00146
Biochemistry 2015, 54, 3660−3669